NANO LETTERS

Letter

Nanowires for Enhanced Boiling Heat Transfer

Renkun Chen, Ming-Chang Lu, Vinod Srinivasan, Zhijie Wang, Hyung Hee Cho, and Arun Majumdar

Nano Lett., **Article ASAP** • DOI: 10.1021/nl8026857

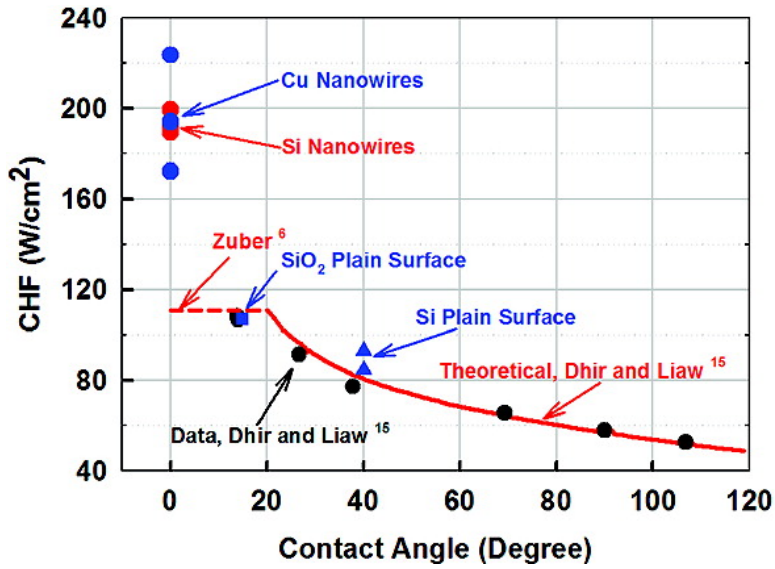

More About This Article

Additional resources and features associated with this article are available within the HTML version:

- Supporting Information
- Access to high resolution figures
- Links to articles and content related to this article
- Copyright permission to reproduce figures and/or text from this article

View the Full Text HTML

NANO LETTERS

XXXX
Vol. xx, No. x
-

Nanowires for Enhanced Boiling Heat Transfer

Renkun Chen,[†,‡] Ming-Chang Lu,[†,‡] Vinod Srinivasan,[†,‡] Zhijie Wang,[‡] Hyung Hee Cho,[§] and Arun Majumdar*[,‡,||]

Department of Mechanical Engineering, University of California, Berkeley, California 94720, School of Mechanical Engineering, Yonsei University, 134 Sinchon-Dong, Seodaemun-gu, Seoul 120-749, Republic of Korea, and Materials Sciences Division, Lawrence Berkeley National Laboratory, Berkeley, California 94720

Received September 3, 2008; Revised Manuscript Received December 2, 2008

ABSTRACT

Boiling is a common mechanism for liquid−vapor phase transition and is widely exploited in power generation and refrigeration devices and systems. The efficacy of boiling heat transfer is characterized by two parameters: (a) heat transfer coefficient (HTC) or the thermal conductance; (b) the critical heat flux (CHF) limit that demarcates the transition from high HTC to very low HTC. While increasing the CHF and the HTC has significant impact on system-level energy efficiency, safety, and cost, their values for water and other heat transfer fluids have essentially remained unchanged for many decades. Here we report that the high surface tension forces offered by liquids in nanowire arrays made of Si and Cu can be exploited to increase both the CHF and the HTC by more than 100%.

The large changes in enthalpy, entropy, and volume during liquid−vapor phase transitions are widely exploited for efficient thermal energy conversion in power generation and refrigeration devices. Boiling is widely used as a liquid−vapor phase transition mechanism in the industry and is also a common phenomenon observed in our daily lives.[1,2] Boiling involves heterogeneous nucleation and growth of vapor bubbles on a heated surface and subsequent departure of these bubbles from the heated surface. The large latent heat of vaporization makes boiling a very efficient mode of heat transfer and is therefore commonly used in many cooling applications, such as in nuclear power plants,[3] high heat flux electronic devices,[4] chemical processes,[5] etc. Pool boiling refers to boiling under natural convection conditions, where the heating surface is submerged in a large body of stagnant liquid and the relative motion of the vapor bubble and its surrounding liquid is primarily due to the buoyancy effect of the vapor.[1,2] Figure 1 qualitatively shows the boiling curve, i.e., the dependence of heat flux, q, on wall superheat, $\Delta T = T_w - T_{sat}$, the temperature difference between the heated surface and the saturation temperature of the liquid (e.g., for water under atmospheric pressure, $T_{sat} = 100$ °C). Up to point A, heat transfer occurs by natural convection and no bubbles are formed. Point A denotes the onset of nucleate boiling whereby vapor bubbles are nucleated at the heated surface. Heat transfer starts to be dominated by partial nucleate boiling (curve A−B), where the wall superheat is sufficiently high to activate discrete bubbles. Beyond point B, nucleate boiling becomes fully developed (curve B−C) as bubbles begin to merge to form columns. At point C, the heat flux reaches its maximum value usually referred to as critical heat flux, or CHF. At this point, the bubbles are large enough to merge and form a continuous vapor film between the liquid and the heated surface. Due to lower thermal conductivity of the vapor compared to the liquid, the thermal resistance increases sharply due to the presence of the vapor film, leading to a large increase in wall superheat from about 20 K at point C to about 1000 K at point E. Therefore, CHF sets the upper limit for safe operation of phase change equipment and is often attributed to the phenomena of nuclear meltdown. Another important parameter in boiling heat

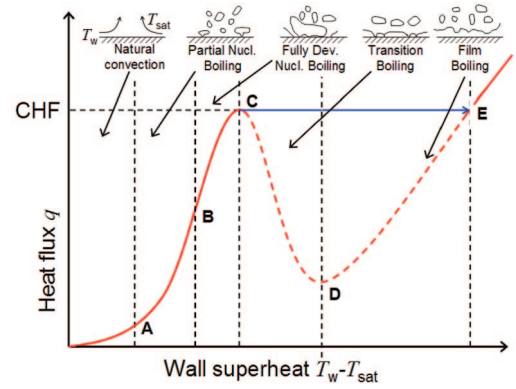

Figure 1. A representative boiling curve qualitatively showing heat flux vs wall superheat $T_w - T_{sat}$ (adapted from ref 1).

* Corresponding author: majumdar@me.berkeley.edu
† These authors contributed equally to this work.
‡ University of California, Berkeley.
§ Yonsei University.
|| Lawrence Berkeley National Laboratory.

10.1021/nl8026857 CCC: $40.75

transfer is heat transfer coefficient (HTC), defined as the heat flux divided by the wall superheat.

Due to the strongly nonlinear nature of the thermofluidic transport processes occurring near the heated surface, there is no consensus on the precise mechanism leading to the establishment of a critical heat flux. One widely known model for the mechanism of CHF developed by Zuber[6] attributes the CHF of boiling on a plain surface to Helmholtz instability of the vapor columns leaving the surface

$$q_{\mathrm{CHF,p}} = \frac{\pi}{24}\sqrt{\rho_{\mathrm{v}}}h_{\mathrm{lv}}[\sigma g(\rho_{\mathrm{l}} - \rho_{\mathrm{v}})]^{1/4} \quad (1)$$

where ρ_{v} is the vapor density, h_{lv} is the latent heat of vaporization, and σ is the surface tension of liquid. From eq 1, the $q_{\mathrm{CHF,p}} \sim 110$ W/cm^2 is obtained for boiling of saturated water at 1 atm, which is close to experimental data.[1,2]

While CHF is considered as the limit for pool boiling, it is not a physical limit, but a practical one. According to kinetic theory, the maximum heat flux that can be attained in a vaporization process would result if all molecules were emitted from the liquid−vapor interface at the speed of sound and without returning to the liquid, i.e., the maximum possible heat flux equals to the flux of molecules multiplied by the mass per molecule and the latent heat,[1] i.e., $q_{\max} = \rho_{\mathrm{v}} c h_{\mathrm{lv}}$, where c is the average speed of vapor molecules. A more rigorous analysis developed by Schrage[7] suggests a proportionality constant of 0.741 placed in front of the right side of the above equation, accounting for the nonequilibrium nature of the interphase mass transfer. For water at atmospheric pressure, $q_{\max}$ is calculated to be 1.65×10^4 W/cm^2 according to Schrage's analysis,[7] which is 2 orders of magnitude higher than the practical CHF of water pool boiling on a plain surface ($\sim$110 W/cm^2).

Pool boiling heat transfer enhancement has been researched extensively over the last 5 decades,[8] which encompassed but was not limited to increasing CHF and/or HTC. A recent comprehensive review of relevant literature has been given by Pioro et al.[8] One common approach is to modify the heating surface condition relevant to boiling, which generally falls in one or several of the following three categories:

(1) Surface modification by increasing surface roughness,[9] coating with microstructures[10] or nanostructures,[11] or using nanoparticle suspension (nanofluids)[12,13] which results in deposition of nanoparticles on the surface, etc. Such modification generally increases surface wettability, which causes an increased CHF through the enhanced liquid spreading over the heated area.[14,15] Another effect of the surface modification is to increase the number of microscale cavities, which serve as the starting sites for heterogeneous nucleation of liquid for bubble formation.[1,2] The relevant sizes of such cavities are generally in the range of tens to hundreds of micrometers.[16]

(2) Increasing the effective heat transfer surface area by thermal fin effect with microfabricated pin−fin structures.[17]

(3) Employing wicking structures to promote the liquid supply to the heated area by capillary pumping, thereby delaying the dry out of the region under the vapor layer.[18,19]

Nanowires, however, represent another class of materials that show properties which could potentially be exploited to promote boiling performance. First, it has been observed that a surface coated with nanowires can be superhydrophilic.[20] Second, nanowire arrays contain many orders of magnitude more cavities and pores compared to any other treated surface using microfabrication or micromachining, thereby effectively increasing the nucleation site density and surface roughness. Furthermore, due to the thermal fin effect, the effective heat transfer area of nanowires may be dramatically higher than that of microfabricated surfaces such as those with micro Si pin fins.[17] Finally, nanowire arrays may act as efficient wicking structures, since the small pores between nanowires provide a very large capillary force, which scales inversely proportionally to the pore size. Due to the above reasons, we hypothesized that CHF and HTC of boiling heat transfer could be enhanced on nanowire arrays. To the best of our knowledge, boiling heat transfer on nanowire arrays has not been reported. Here we report our experimental work on pool boiling of saturated water on surfaces covered with dense arrays of nanowires made by either Si or Cu. As we shall see later, for both Si and Cu nanowires, the CHF and HTC were observed to increase significantly, compared to the boiling on plain surface. The CHF reported here ($\sim$200 W/cm^2) is one of the highest reported CHF values of boiling heat transfer.

Si nanowires were synthesized by a wafer scale aqueous electroless etching (EE) technique.[21] These nanowires were prepared by immersing a Si wafer into an aqueous solution of $AgNO_3$ and HF acid. On the wafer surface, Ag^+ reduces to Ag by oxidizing the surrounding Si lattice, which is subsequently etched by HF. Initial reduction of Ag^+ forms Ag nanoparticles, which define the spatial region of the following oxidation and etching process. After continuous process of oxidation and etching, the unetched region forms nanowire arrays. Si nanowires synthesized by this technique are vertically aligned and have diameters in the range of 20−300 nm. In the present study, nanowires approximately 40−50 μm long were synthesized for the boiling experiments. Panels a and b of Figure 2 show scanning electron microscopy (SEM) micrographs of the top view and cross section of Si nanowire arrays used in the present study, respectively.

Cu nanowires were synthesized by electroplating of Cu into nanoscale pores of commercially available porous alumina membranes (Whatman Inc.).[22] In the present study, membranes 25 mm in diameter and 60 μm thick with 200 nm nominal pore size and approximately 50% nominal porosity were used as the templates for Cu electroplating, the obtained nanowires (Figure 2, panels c and d) are approximately 200 nm in diameter and 40−50 μm long and with 50% filling ratio. After Cu nanowires were deposited, the membrane was bonded to a Si substrate and the alumina template was removed by etching in NaOH solution to obtain free-standing Cu nanowires (see Figure S1 in Supporting Information for details).

It is worth mentioning that there are microscale defects naturally formed within the nanowire arrays, as shown in

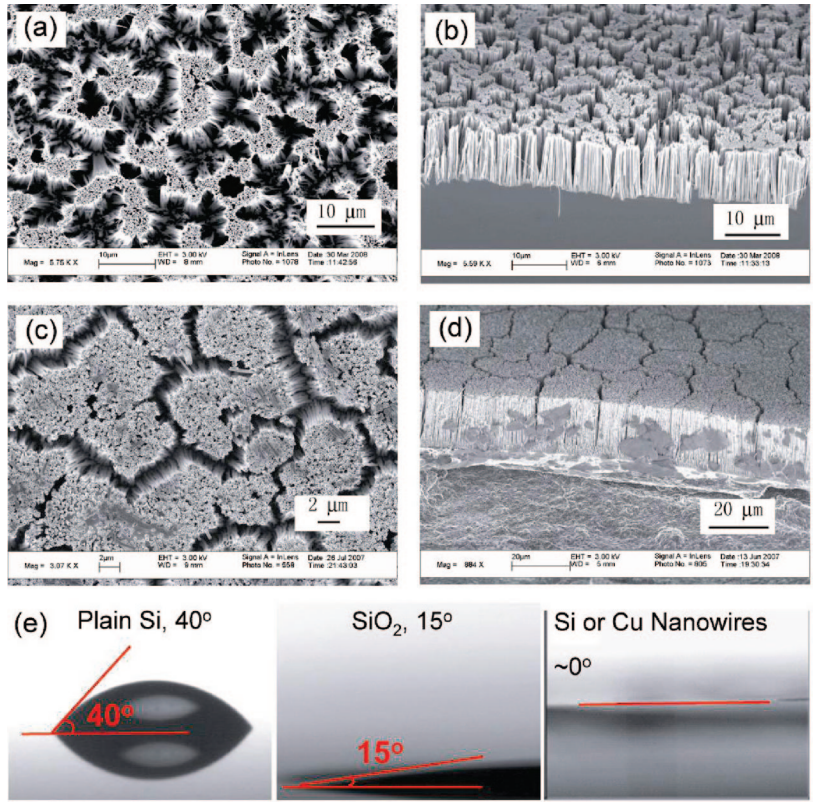

Figure 2. Scanning electron microscopy (SEM) graphs of (a) top view of Si Nanowires, (b) cross section of Si Nanowires, (c) top view of Cu Nanowires, (d) cross section of Cu nanowires, (e) static contact angles of a water droplet on surfaces of Si, SiO_2, and Si and Cu nanowires.

Figure 2a−d. The formation of these cavities is presumably due to the surface tension of water during the drying process of nanowire synthesis, which pulls nanowires together to form bundles of wires and microscale cavities between them. As we shall see later, such microscale cavities are ideal as active sites for bubble formation during boiling.

In order to reach CHF for boiling with water, a heater with heat flux up to several hundred W/cm^2 is required. The heater used in this study is a thin layer of indium tin oxide (ITO), deposited on the back side of a Si substrate, on which either the Si nanowires were synthesized or the Cu nanowire arrays were bonded, as illustrated in Figure 3a. Heat flux up to 300 W/cm^2 can be produced on the 1 cm × 1 cm ITO film by Joule heating of direct current supplied via two patterned Cu electrodes. Since the heater is chemically bonded to the Si wafer that served as the substrate for nanowire arrays, the thermal resistance between the heater and the heating surface is minimized, compared to the interface resistance if thermal epoxy were used. The test sample including Si substrate with nanowires and heater was mounted to a Teflon block (thermal conductivity 0.2 W/(m K)) to ensure thermal insulation (see Figure S2 in Supporting Information).

To perform the boiling experiment, the whole test assembly was immersed into a pool of deionized (DI) water, which was then heated up to its saturation temperature (100 °C) at 1 atm. Throughout the whole experiment, the temperature of the ambient water was continuously monitored by a T type thermocouple to ensure it was at 100 °C. After the pool of water is maintained at 100 °C for at least 30 min, power was supplied to the ITO heater incrementally to

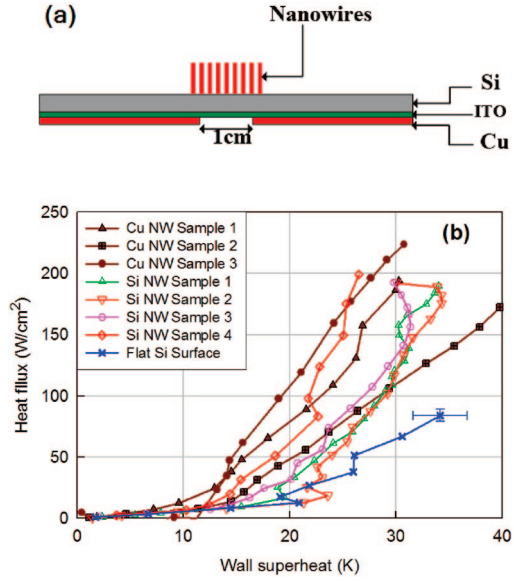

Figure 3. Boiling heat transfer experiment: (a) schematic of the test sample assembly; (b) boiling curves for plain Si surface, Si nanowires, and Cu nanowires.

heat up the Si substrate. The temperature of the heater was measured by two T type thermocouples attached to it. The critical heat flux (CHF) was postulated to be equal to the heating power corresponding to the last observed stable temperature, beyond which a sudden dramatic increase in heater temperature was observed.

Figure 3b depicts the boiling curves of plain Si surface and Si and Cu nanowires. Boiling on plain Si surface served

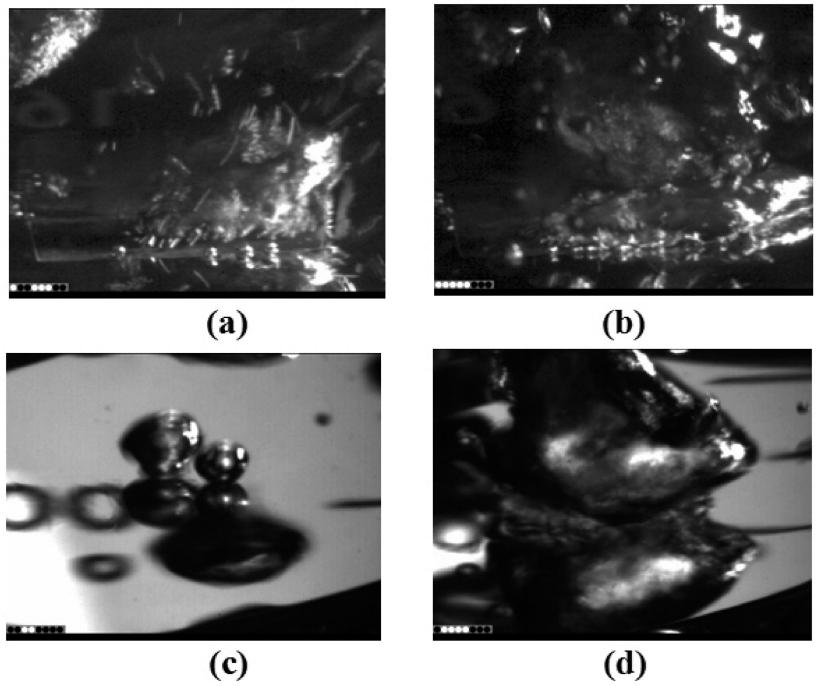

Figure 4. Bubble images: (a) Si nanowires, 18 W/cm^2; (b) Si nanowires, 177 W/cm^2; (c) Si, 20 W/cm^2; (d) Si, 93 W/cm^2.

as the primary control for the boiling performance comparisons. The error bar shown in the plain Si boiling curve represents the range of CHF and wall superheat at CHF on multiple samples. CHF and HTC for plain Si were found to be 82 $\pm$ 5.0 W/cm^2 and 2.64 $\pm$ 0.14 W/(cm^2 K), respectively. The boiling results on the Si surface presented here are consistent with experimental results reported in the literature for a plain surface, e.g., by Theofanous et al.[23] Boiling curves of Si and Cu nanowires appear to be similar to each other, although the thermal conductivities for Cu and Si nanowires are dramatically different (400 W/(m K) for Cu and ~10 W/(m K) for EE Si nanowires[21]). This is reasonable as heat transfer in boiling is dominated by bubble dynamics[1,2] rather than heat conduction, and the similar boiling behavior is a result of similar morphologies of Si and Cu nanowire arrays. For both Si and Cu nanowires, the CHF is 192 $\pm$ 1.3 and 197 $\pm$ 21 W/cm^2, respectively, while HTC values are 6.00 $\pm$ 1.23 and 6.15 $\pm$ 0.40 W/(m K), respectively, in the wall superheat range of 10−30 K. Both CHF and HTC of nanowires are more than doubled compared to plain Si. The CHF reported here (~200 W/cm^2) is among the highest reported CHF values.

The significant enhancement of HTC of nanowires compared to plain surface could be attributed to the following reasons, as we initially anticipated. As shown in Figure 2a−d, there are numerous naturally formed defects of several micrometers between the Si or Cu nanowires. In the present study, it can be calculated that the size range of active cavities is from 1 to 6 μm when the wall superheat is below 30 K (see Figure S3 in Supporting Information). Therefore, these cavities are likely to be active cavity sites for heterogeneous nucleation, and more nucleation sites formed between nanowires could result in a higher HTC. This can be further demonstrated by the bubble images as shown in Figure 4, which exhibits that more bubbles were produced for Si nanowires compared to plain Si surface under both moderate heat flux (~20 W/cm^2) and heat flux close to CHF (177 W/cm^2 for Si nanowires and 93 W/cm^2 for plain Si).

The enhanced CHF could also be attributed to some unique properties of nanowires. One plausible mechanism is the increased surface wettability. The nearly zero apparent contact angle of water on the nanowire arrays suggests that the nanowire arrays are superhydrophilic (see Figure 2e), which is expected to result in a higher CHF. Earlier studies suggest that nanowire arrays can be superhydrophilic (e.g., Si nanowires with native oxide[20] and TiO_2 nanotubes[24]) or superhydrophobic (e.g., carbon nanotubes arrays[25]). For a rough surface such as the one covered by nanowire arrays in the present study, there are typically two equilibrium states in which a drop resides:[26] the drop either wets the grooves (Wenzel state) or sits on the peaks of the rough surface (Cassie drop). The superhydrophilicity of our nanowire arrays can be explained with the Wenzel equation ($\cos\theta = r\cos\theta'$, where θ and θ' are contact angles on the roughened (roughness factor = r) and completely smooth surfaces, respectively). This equation indicates that the surface roughness enhances the hydrophilicity of hydrophilic surfaces ($\theta < 90°$) and enhances the hydrophobicity of hydrophobic ones ($\theta > 90°$) because r is always larger than 1. The water contact angle of a flat Si or Cu surface is less than 90° due to native oxides formed on the surface, so the roughened surfaces (nanowire arrays) become more hydrophilic in the present study. In the case of superhydrophobicity, it may be explained in terms of the Cassie equation.[25] Figure 5 presents the contact angle dependence of CHF. In general, CHF increases as contact angle decreases.[15] To confirm the effect of surface wettability, CHF of pool boiling on a Si substrate coated with a SiO_2 layer was measured and compared against

the native Si surface. The contact angles for Si and SiO_2 surfaces are 40° and 15°, respectively (Figure 2e). The SiO_2 surface shows a higher CHF (107 W/cm^2) compared to plain Si, as shown in Figure 5, which is consistent with Dhir and Liaw's model and experimental data.[15]

However, this alone does not explain the extremely high CHF observed for nanowires. According to Dhir and Liaw,[15] CHF for a zero contact angle surface is given by Zuber's model[6] and is calculated to be 110 W/cm^2 according to eq 1, which is still significantly below the observed CHF on Si and Cu nanowires (see Figure 5). However, Zuber's model[6] does not include surface conditions and is only applicable to a plain surface. For a surface coated with microstructures, such as the microcavities in nanowires studied here, there are two possible mechanisms for CHF:[18] the hydrodynamic limit originally proposed by Zuber[6] but extended to a surface with microstructure coating and the capillary limit. As discussed earlier, the onset of CHF based on the hydrodynamic limit $q_{CHF,h}$ is due to the instability of vapor columns. The microsized cavities in the nanowire arrays could provide sites for stable vapor formation at the top of the nanowire coating, which alter the critical distance between vapor columns on the heating surface and thus adjust the critical instability wavelength. By extending Zuber's model, $q_{CHF,h}$ for a surface with microscale coating can be estimated using the following equation[27]

$$\frac{q_{CHF,h}}{q_{CHF,p}} = \sqrt{\frac{\lambda_p}{\lambda_\mu}} \qquad (2)$$

where λ_p and λ_μ are the critical instability wavelengths on a plain surface and a surface with microscale coating, respectively. According to Zuber's model[6]

$$\lambda_p = 9[/g(\rho_l - \rho_v)]^{1/2}$$

Polezhaev and Kovalev[27] suggested

$$\lambda_\mu = \left(\frac{\pi}{5.88\varphi_w^{2.8}}\right)^2 d_{br}$$

where φ_p is the porosity of the *whole* nanowire array and is taken to be 0.4 and d_{br} is the diameter of the breakthrough bubbles, which are the starting bubbles penetrating through the nanowire array. Without visual verification on bubble formation, d_{br} is assumed to be 10 μm based on the microscale cavities formed in nanowire arrays as shown in Figure 2. The obtained $q_{CHF,h}$ is nearly 1258 W/cm^2. The other mechanism for CHF is due to the capillary pumping limit. The Si and Cu nanowires having characteristic diameter (d) around 20−300 and 200 nm, respectively, provide a large capillary pumping force to bring liquid back to the heated surface, and thereby prevent the drying out of the heated area and delay the onset of CHF. The CHF due to the capillary limit ($q_{CHF,c}$) can be estimated by the balance between the capillary pumping force and the liquid viscous drag along its flow path[18]

$$\frac{q_{CHF,c}}{0.53(\rho_l \sigma h_{lv}/\mu_l)((K\phi_s)^{1/2}/D)} = 1 - \frac{C_E}{0.53}\frac{D}{\sqrt{\phi_s}}\frac{q_{CHF,c}^2}{\rho_l \sigma h_{lv}^2} \qquad (3)$$

where μ_l is the viscosity of the liquid, K is the permeability of the wicking structure, C_E is the Ergun coefficient,[28] D is the liquid flow distance, and φ_s is the porosity of nanowire *subarray*, representing *each bundle* of nanowires separated by the microscale cavities. The Carmen−Kozeny model[28] is used to calculate the permeability which results in $K = \varphi_s d^2/[180(1-\varphi_s)^2]$ and $C_E = (0.018/\varphi_s^3)^{1/2}$. The characteristic diameter of d = 200 nm, liquid flow distance of D = 50 μm, and *subarray* porosity φ_s = 0.1 are assumed in the present study based on SEM images of nanowires (Figure 2 a−d). Note φ_s is different from φ_w used in eq 2, which is the porosity of the *whole* nanowire array. The $q_{CHF,c}$ given by eq 3 is approximately 250 W/cm^2. From the above analysis, it is shown that the capillary limit $q_{CHF,c}$ is lower than the hydrodynamic limit $q_{CHF,h}$ and is believed to be the dominant mechanism for the observed CHF in nanowires. The estimated $q_{CHF,c}$ agrees well with our experimental data. In principle, $q_{CHF,c}$ could be further increased by taking the advantage of large capillary force of nanowire array with proper design for liquid flow passages in the nanowire arrays to minimize the flow resistance.

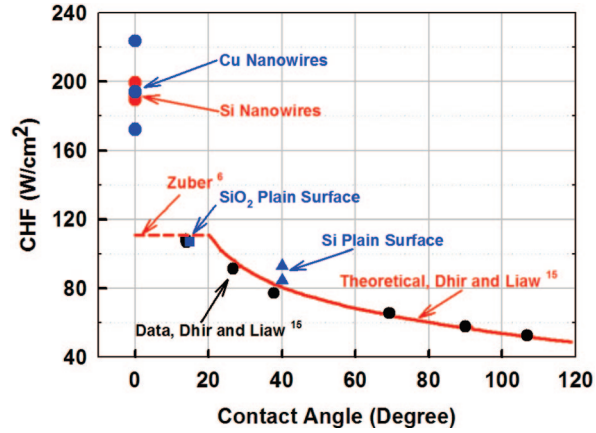

Figure 5. Dependence of CHF on contact angle. CHF of plain Si (blue triangle) and SiO_2 (blue rectangle) observed in the present study follows the theoretical models given by Dhir and Liaw[15] (red solid line) and Zuber[6] (red dashed line) and experimental data of Dhir and Liaw[15] (black circles). However, CHF values for Cu and Si nanowires (blue and red circles, respectively) are significantly higher than the theoretical prediction, indicating mechanism besides contact angle dependence is also involved.

An interesting phenomenon was observed in the boiling curves of Si nanowires (samples 2 and 3), where the wall superheat decreased when heat flux approached the CHF. This phenomenon can be attributed to the activation of submicrometer cavities in the Si nanowire arrays. The superheat needed to activate these cavities as nucleation sites is higher than 30 K (see Figure S3 in Supporting Information). When the heat flux approached CHF, the wall superheat is 30 K or higher. Therefore, a large amount of submicrometer cavities can be activated and more bubbles are produced, resulting in a sudden increase in HTC and, consequently, decrease in wall superheat near the CHF. The phenomenon was not observed in Cu nanowires, presumably due to the fact that there are fewer submicrometer cavities formed in Cu nanowires, as evident in SEM images in Figure 2. This phenomenon also suggests a possible route to further increase the HTC for pool boiling by creating optimal cavity sites of different length scales corresponding to various wall superheats, which is what we are pursuing currently.

In summary, we report the first study on pool boiling of saturated water on nanowires, made of Si or Cu, and observe significant enhancement of both critical heat flux and thermal conductance on nanowires compared to plain surface. The reported CHF ($\sim$200 W/cm^2) is among the highest values for pool boiling heat transfer. Such enhancement can be attributed to some unique properties of nanowires, such as high nucleate site density, superhydrophilicity, and enhanced capillary pumping effect. The insight obtained from this study indicates that further enhancement of CHF and HTC is possible by rational design and synthesis of nanowire arrays. The techniques employed here for large scale nanowire synthesis (electrochemical etching and electroplating) are inexpensive and readily scalable for large area fabrication; hence the present study could lead to practical applications involving thermal management and energy conversion of high heat flux.

Acknowledgment. This work was supported by Intel Corporation and a grant from the UC Discovery Program. We thank the UC Berkeley Microfabrication Laboratory for the use of their facilities. The authors thank Allon I. Hochbaum and Professor Peidong Yang for the help and discussion on EE Si Nanowire synthesis and Brian Bush and Professor Roya Maboudian for the discussion on Cu electroplating. We acknowledge Professor Van P. Carey as well as Dr. Ravi Prasher and his colleagues at Intel for helpful discussion on boiling heat transfer.

Supporting Information Available: Experimental details on Cu nanowire synthesis and bonding, boiling experimental setup and data reduction, and a plot of size range of active nucleation cavities. This material is available free of charge via the Internet at http://pubs.acs.org.

References

(1) Carey, V. P. *Liquid-Vapor Phase-Change Phenomena*; Hemisphere: Washington, DC, 1992.
(2) Dhir, V. K. *Annu. Rev. Fluid Mech.* **1998**, *30*, 365–401.
(3) Kang, M. G. *Ann. Nucl. Eng.* **1998**, *25*, 295–304.
(4) Mudawar, I. *IEEE Trans. Compon. Packag. Technol.* **2001**, *24*, 122–141.
(5) Thome, J. R. *Enhanced Boiling Heat Transfer*; Hemisphere: New York, 1990.
(6) Zuber, N. *Hydrodynamic Aspects of Boiling Heat Transfer*; AEC Report AECU-4439, June **1959**.
(7) Schrage, R. W. *A Theoretical Study of Interphase Mass Transfer*; Columbia University Press: New York, 1953.
(8) Pioro, I. L.; Rohsenow, W.; Doerffer, S. S. *Int. J. Heat Mass Transfer* **2004**, *47*, 5033–5044.
(9) Kurihara, H. M.; Myers, J. E *AIChE J.* **1960**, *6*, 83–91.
(10) Chang, J. Y.; You, S. M. *Int. J Heat Mass Transfer* **1997**, *40*, 4437–4447.
(11) Li, C.; Wang, Z.; Wang, P. I.; Peles, Y.; Koratkar, N.; Peterson, G. P. *Small* **2008**, *4*, 1084–1088.
(12) You, S. M.; Kim, J. H.; Kim, K. H. *Appl. Phys. Lett.* **2003**, *83*, 3374–3376.
(13) Kim, S. J.; Bang, I. C.; Buongiorno, J.; Hu, L. W. *Appl. Phys. Lett.* **2006**, *89*, 153107.
(14) Wang, C. H.; Dhir, V. K. *J. Heat Transfer* **1993**, *115*, 659–669.
(15) Dhir, V. K.; Liaw, S. P. *J. Heat Transfer* **1989**, *111*, 739–746.
(16) Hsu, Y. Y. *J. Heat Transfer* **1962**, 207–216.
(17) Wei, J. J.; Honda, H. *Int. J. Heat Mass Transfer* **2003**, *46*, 4059–4070.
(18) Liter, S. G.; Kaviany, M. *Int. J. Heat Mass Transfer* **2001**, *44*, 4287–4311.
(19) Li, C.; Peterson, G. P. *J. Heat Transfer* **2007**, *129*, 1465–1475.
(20) Yuan, J.; Liu, X.; Akbulut, O.; Hu, J.; Suib, S. L.; Kong, J.; Stellacci, F. *Nat. Nanotechnol.* **2008**, *3*, 332–336.
(21) Hochbaum, A. I.; Chen, R.; Delgado, R. D.; Liang, W.; Garnett, E. C.; Najarian, M.; Majumdar, A.; Yang, P. D. *Nature* **2008**, *451*, 163–167.
(22) Gao, T.; Meng, G.; Wang, Y.; Sun, S.; Zhang, L. *J. Phys.: Condens. Matter* **2002**, *14*, 355–363.
(23) Theofanous, T. G.; Tu, J. P.; Dinh, A. T.; Dinh, T. N. *Exp. Therm. Fluid Sci.* **2002**, *26*, 775–792.
(24) Miyauchi, M.; Tokudome, H *J. Mater. Chem.* **2007**, *17*, 2095–2100.
(25) Lau, K. K. S.; Bico, J.; Teo, K. B. K.; Chhowalla, M.; Amaratunga, G. A. J.; Milne, W. I.; McKinley, G. H.; Gleason, K. K. *Nano Lett.* **2003**, *3*, 1701–1705.
(26) Patankar, N. A. *Langmuir* **2004**, *20*, 7097–7102.
(27) Polezhaev, Y. V.; Kovalev, S. A. *Therm. Eng.* **1990**, *37*, 617–620.
(28) Kaviany, M. *Principles of Heat Transfer in Porous Media*; Springer: New York, 1999.

NL8026857